

Learning Multi-Agent Coordination through Connectivity-driven Communication

Emanuele Pesce¹ and Giovanni Montana^{1*}

¹WMG, University of Warwick, Coventry, CV4 7AL, UK.

*Corresponding author(s). E-mail(s): g.montana@warwick.ac.uk;
Contributing authors: e.pesce@warwick.ac.uk;

Abstract

In artificial multi-agent systems, the ability to learn collaborative policies is predicated upon the agents' communication skills: they must be able to encode the information received from the environment and learn how to share it with other agents as required by the task at hand. We present a deep reinforcement learning approach, Connectivity Driven Communication (CDC), that facilitates the emergence of multi-agent collaborative behaviour only through experience. The agents are modelled as nodes of a weighted graph whose state-dependent edges encode pair-wise messages that can be exchanged. We introduce a graph-dependent attention mechanisms that controls how the agents' incoming messages are weighted. This mechanism takes into full account the current state of the system as represented by the graph, and builds upon a diffusion process that captures how the information flows on the graph. The graph topology is not assumed to be known *a priori*, but depends dynamically on the agents' observations, and is learnt concurrently with the attention mechanism and policy in an end-to-end fashion. Our empirical results show that CDC is able to learn effective collaborative policies and can over-perform competing learning algorithms on cooperative navigation tasks.

Keywords: Reinforcement Learning, Multi-agent system, Neural Networks, Graphs

1 Introduction

In reinforcement learning (RL), an agent learns to take sequential decisions by mapping its observations of the world to actions using a reward as feedback signal [1]. In the last years, deep artificial neural networks [2, 3] have been leveraged to improve the learning ability of RL algorithms in a number of ways, e.g. as policy function approximators to map observations to actions. The resulting deep reinforcement learning algorithms (DRL) have recently achieved unprecedented performance in single-agent tasks, e.g. in playing Go [4] and Atari [5, 6] games.

Multi-agent reinforcement learning (MARL) extends RL to problems characterized by the interplay of multiple agents operating in a shared environment. This is a scenario that is typical of many real-world applications including robot navigation [7], autonomous vehicles coordination [8], traffic management [9], and supply chain management [10]. Compared to single-agent systems, MARL presents additional layers of complexity. When multiple learners interact with each other, the environment becomes highly non-stationary from the point of view of each individual actor [11]. Moreover, credit assignment [12], which is the ability to determine how the actions of each individual agent impact on the overall system performance, becomes particularly difficult [13–15].

We are interested in systems involving agents that autonomously learn how to collaborate in order to achieve a shared outcome. When multiple agents are expected to develop a cooperative behaviour, an important need emerges: an adequate communication protocol must be established to support the level of coordination that is necessary to solve the task. The fact that communication plays a critical role in achieving synchronization in multi-agent systems has been extensively documented [16–23]. Building upon this evidence, a number of multi-agent DRL algorithms (MADRL) have been developed lately which try to facilitate the spontaneous emergence of communication strategies during training. In particular, significant efforts have gone into the development of attention mechanisms for filtering out irrelevant information [24–30] (see also Section 4).

In this paper we introduce a MADRL algorithm for cooperative multi-agent tasks. Our approach relies on learning a state-dependent communication graph whose topology controls what information should be exchanged within the system and how this information should be distributed across agents. As such, the communication graph plays a dual role. First, it represents how every pair of agents jointly encodes their observations to form local messages to be shared with others. Secondly, it controls a mechanism by which local messages are propagated through the network to form agent-specific information content that is ultimately used to make decisions. As we will demonstrate, this approach supports the emergence of a collaborative decision making policy. The core idea we intend to exploit is that, given any particular state of the environment, the graph topology should be self-adapting to support the most

efficient flow of information. This raises the question: how should efficiency be measured?

Our proposed approach, *connectivity-driven communication* (CDC), is inspired by the process of heat transference over networks, and specifically the heat kernel (HK). The HK describes the effect of applying a heat source to a network and observing the diffusion process over time. As such, it can be used to characterise the way in which the information flows across nodes. The HK has been used in a number of different application domains where there is a need to characterise the topology of graph, e.g. in 3D object recognition [31] and neuroimaging [32, 33]. Various metrics obtained from the HK have been used to organise the intrinsic geometry of a network over multiple-scales by capturing local and global shapes' in relation to a node via a time parameter. The HK also incorporates a concept of node influence as measured by heat propagation in a network, which can be exploited to characterise how efficiently the information propagates between any pair of nodes. To the best of our knowledge, this is the first time that the HK has been used to develop an end-to-end learnable attention mechanism enabling multi-agent cooperation.

Our approach relies on an actor-critic paradigm [34–36] and is intended to extend the centralized-learning with decentralized-execution (CLDE) framework [20, 37]. In CDC, all the observations from each agent are assumed known only during the training phase whilst during execution each agent makes autonomous decisions using only their own information. The entire model is learned end-to-end supported by the fact that the heat-kernel is a differentiable operator allowing the gradients to flow throughout the architecture. The performance of CDC has been evaluated against alternative methods on four cooperative navigation tasks. Our experimental evidence demonstrates that CDC is capable of outperforming other relevant state-of-the-art algorithms. In addition, we analyse the communication patterns discovered by the agents to illustrate how interpretable topological structures can emerge in different scenarios.

The structure of this work is as follows. In Section 2 we discuss related state-of-the-art MADRL methods focusing on cooperating systems with communication mechanisms. In Section 3 we provide the details of the proposed CDC algorithm; additional technical details can be found in the Appendix. Experimental results are then provided in Section 4. Finally, in Section 5, we discuss the benefits and potential limitations of the proposed methodology with a view on further improvements in future work.

2 Related Work

Multi-agent systems have been widely studied in a number of different domains, such as machine learning [38], game theory [39] and distributed systems [40]. Recent advances in deep reinforcement learning have allowed multi-agent systems capable of autonomous decision-making [41–43] improving

tabular-based solutions [44]. In this section, we briefly review recent developments in MADRL with a focus on communication strategies that have been proposed to improve cooperation.

2.1 Centralised learning with decentralised execution

When multiple learners interact with each other, the environment becomes non-stationary from the perspective of individual agents which results in increased training instability [45, 46]. An approach that has proved particularly effective consists of training the agents assuming centralised access to the entire system’s information whilst executing the policies in a decentralised manner (CLDE) [20, 23, 29, 37, 47, 48]. During training, a critic module has access to information related to other agents, i.e. their actions and observations. MADDPG [37], for example, extends DDPG [35] in this fashion: each agent has a centralised critic providing feedback to the actors, which decide what actions to take. A variant of this approach has recently been proposed to deal with partially observable environments through the use of recurrent neural networks [49, 50]. In [48], a centralised critic is used to estimate the Q-function whilst decentralised actors optimise the agents’ policies. In [51], an action-value critic network coordinates decentralised policy networks for a fleet management problem.

2.2 Communication methods

Communication has always played a crucial role in facilitating synchronization and coordination [52–56]. Some of the recent MADRL approaches facilitate the emergence of novel communication protocols through implicit communication. For example, in CommNet [21], the hidden states of an agent’ neural network are first averaged and then used jointly with the agent’s own observations to decide what action to take. Similarly, in [57], communication is enabled by connecting agents’ policies through a bidirectional recurrent neural network that can produce higher-level information to be shared. In IC3Net [22], a gating mechanism decides whether to allow or block access to other agents’ hidden states.

Other approaches have introduced explicit communication mechanisms that can be learnt from experience. For instance, in RIAL [20], each agent learns a simple encoding that is transferred over a differentiable channel and allows the gradient of the Q-function to flow; this enables an agent’s feedback to take into account the exchanged information. In our previous work, [23], the agents are equipped with a memory device allowing them to write and read signals to be shared within the system. The communication mechanism we propose in this paper is also explicit; messages are signals that must be shared within the system in order to maximize the shared rewards and serve no other purpose.

2.3 Attention mechanisms to support communication

In a collaborative decision making context, attention mechanisms are used to selectively identify relevant information coming from the environment and other agents that should be prioritised to infer better policies. For example, in [24], the agents first encode their observations to produce messages; then an attention unit, implemented as a recurrent neural network (RNN), probabilistically controls which incoming messages are used as inputs for the action selection network. The CommNet algorithm [21] has been extended using a multi-agent predictive modeling approach [27] which captures the locality of interactions and improves performance by determining which agents will share information. The TarMac algorithm [28] instead leverages the signature-based attention model originally proposed in [58]. Here, each agent receives the messages broadcasted by others and produces a query that helps select what information to keep and what to discard. The latter approach is closely related to the work proposed in this paper; ours agents also aggregate information coming from different sources in order to maximise their final reward.

2.4 Diffusion processes on graphs

Spectral graph theory allows to relate the properties of a graph to its spectrum by analysing its associated eigenvectors and eigenvalues [59–61]. The heat kernel falls in this category; it is a powerful and well-studied operator allowing to study certain properties of a graph by solving the heat diffusion equation. The HK is determined by exponentiating the graph’s Laplacian eigensystem [62] over time. The resulting features can be used to study the graph’s topology and have been utilised across different applications whereby graphs are naturally occurring data structures; e.g. the HK has been used for community detection [63], data manifold extraction [64], network classification [33] and image smoothing [31] amongst others. In recent work, the HK has been adopted to extend graph convolutional networks [65] and define edge structures supporting convolutional operators [66]. In this work, we use the HK to characterise the state-dependent topology of a multi-agent communication network and learn how the information should flow within the network.

2.5 Graph-based communication mechanisms

Graph structures provides a natural framework for modelling interactions in RL domains [67–69]. Lately, Graph Neural Networks (GNNs) have also been adopted to learn useful graph representations in cooperative multi-agent systems [70–74]. For example, graphs have been used to model spatio-temporal dependencies within episodes for traffic light control [75], and to infer a multi-agent connectivity structure which, once processed by a GNN, generates the features required to decide what action to take [76–78]. Heterogeneous graph attention networks [79] have been introduced to learn efficient and diverse communication models for coordinating heterogeneous agents. Graph

convolutional networks capturing multi-agent interactions have also been combined with a counterfactual policy gradient algorithm to deal with the credit assignment problem [80].

GNNs have also supported the development of multi-stage attention mechanisms. For instance, [26] describe a two-stage approach whereby multi-agent interactions are first determined, and their importance is then estimated to generate actions. In GraphComm [81], the agents share their encoded observations over a multi-step communication process; at each step a GNN processes a graph and generates signals for the subsequent communication round. This multi-round process is designed to increase the length of the communication mechanism and favour a longer range exchange of information. The MAGIC algorithm [82] consists of a scheduled learning when to communicate and whom to address messages to, and a message processor to process communication signals; both components have been implemented using GNNs and the entire architecture is learned end-to-end.

In our proposed model, the attention mechanism depends on how the encoded information exchanged amongst the agents flows within the graph; the graph topology itself depends on the encoded observations and the heat kernel is used as a topology-dependent feature to control the agent’s communication. In our approach, the process of encoding the observations, inferring the graph topology, and learning the attention mechanism are all coupled with the aim to learn an effective policy.

3 Connectivity-driven Communication

3.1 Problem setting

We consider Markov Games, partially observable extension of Markov decision processes [83] involving N interacting agents. We use \mathcal{S} to denote the set of environmental states; \mathcal{O}_i and \mathcal{A}_i indicate the sets of all possible observations and actions for the i^{th} agent, with $i \in 1, \dots, N$, respectively. The agent-specific (private) observations at time t are denoted by $\mathcal{O}_i^t \in \mathcal{O}_i$, and each action $a_i^t \in \mathcal{A}_i$ is deterministically determined by a mapping, $\mu_{\theta_i} : \mathcal{O}_i \mapsto \mathcal{A}_i$, which is parametrised by θ_i . A transition function $\mathcal{T} : \mathcal{S} \times \mathcal{A}_1 \times \mathcal{A}_2 \times \dots \times \mathcal{A}_N$ describes the stochastic behaviour of the environment. Each agent receives a reward, defined as a function of states and actions $r_i : \mathcal{S} \times \mathcal{A}_1 \times \mathcal{A}_2 \times \dots \times \mathcal{A}_N \mapsto \mathbb{R}$ and learns a policy that maximises the expected discounted future rewards over a period of T time steps, $J(\theta_i) = \mathbb{E}[R_i]$, where $R_i = \sum_{t=0}^T \gamma^t r_i^t(s^t, a_1^t, \dots, a_N^t)$ is the discounted sum of future rewards, where $\gamma \in [0, 1]$ is the discount factor.

3.2 Learning the dynamic communication graph

We model each agent as the node of a time-depending, undirected (and unknown) weighted graph, $G^t = (V, \mathbf{S}^t)$, where V is a set of N nodes and \mathbf{S}^t is an $N \times N$ matrix of edge weights. Each $\mathbf{S}^t(u, v) = \mathbf{S}^t(v, u) = s_{u,v}^t$ quantifies the degree of communication or connectivity strength between a given pair of

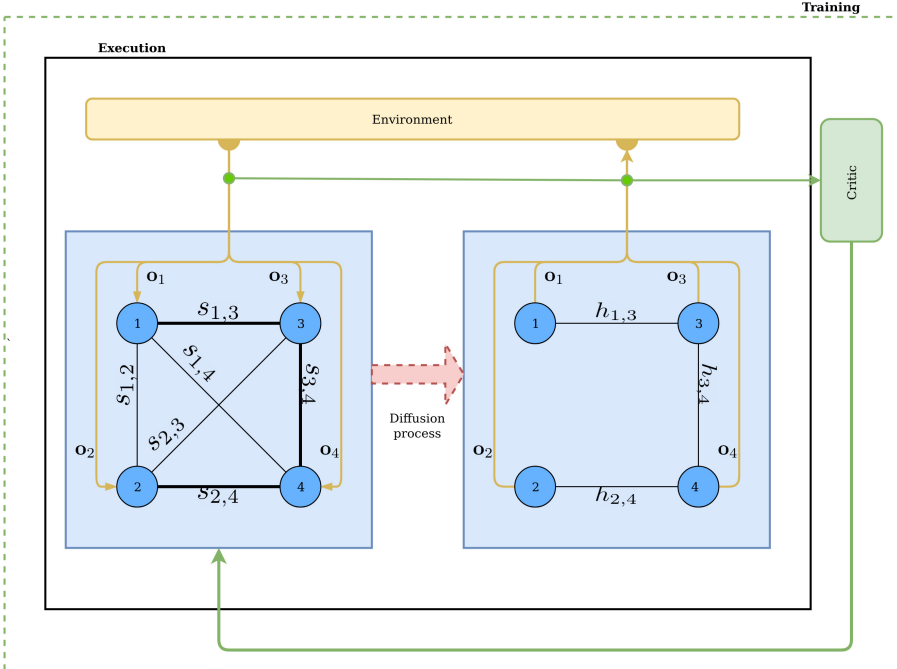


Fig. 1: Diagrammatic representation of CDC at a fixed time-step. Agents' observations are encoded to generate a graph topology (blue box on the left). The diffusion process is used to quantify global information flow throughout the graph and to control the communication process (blue box on the right). In this example, the line thickness is proportional to communication strength. At training time, observations and actions are utilised by the critic to receive feedback on the graph components.

agents, u and v . Specifically, we assume that each $s_{u,v}^t \in [0, 1]$ with values close to 1 indicating strong connectivities, and to 0 a lack of connectivity.

In our formulation, each $s_{u,v}^t$ is not known *a priori*. Instead, each one of these connectivities is assumed to be a time-dependent parameter that varies as a function of the current state of the environment. This is done through the following two-step process. First, given a pair of agents, u and v , their private observations at time-step t are encoded to form a local message,

$$\mathbf{c}_{u,v}^t = \mathbf{c}_{v,u}^t = \varphi_{\theta^c}(\mathbf{o}_u^t, \mathbf{o}_v^t) \quad (1)$$

where φ_{θ^c} is a non-linear mapping modelled as a neural network with parameter θ^c . Each local message is then encoded non-linearly to produce the corresponding connectivity weight,

$$s_{u,v}^t = s_{v,u}^t = \sigma(\varphi_{\theta^s}(\mathbf{c}_{u,v}^t)) \quad (2)$$

where φ_{θ^s} is a neural network parameterised by θ^s and σ is the sigmoid function.

3.3 Learning an time-dependent attention mechanism

Once the time-dependent connectivities in Eq. 2 are estimated, the communication graph G^t is fully specified. Given this graph, our aim is to characterise the relative contribution of each node to the overall flow of information over the entire network, and let these contributions define a attention mechanism controlling what messages are being exchanged. The resulting attention mechanism should be differentiable with respect to the network parameters to ensure that, during backpropagation, all the gradients correctly flow throughout the architecture to enable end-to-end training.

Our observation is that a diffusion process over graphs can be deployed to quantify how the information flows across all agents for any given communication graph, G^t . The information flowing process is conceptualised as the amount of energy that propagates throughout the network [84]. Specifically, we deploy the heat diffusion process: we mimic the process of applying a source of heat over a network and observe how it varies as a function of time. In our context, the heat transfer patterns reflect how efficiently the information propagates at time t .

First, we introduce a diagonal matrix $\mathbf{D}(u)$ of dimension $N \times N$ with diagonal elements given by

$$D(u, u) = \sum_{v \in V} s_{u,v}, \quad \forall u \in V.$$

Each such element provides a measure of strength of node u . The Laplacian of the communication graph G is given by

$$\mathcal{L} = \mathbf{D} - \mathbf{S}$$

and its normalised version is defined as

$$\hat{\mathcal{L}} = \frac{1}{\sqrt{\mathbf{D}}} \mathcal{L} \frac{1}{\sqrt{\mathbf{D}}}. \quad (3)$$

The differential equation describing the heat diffusion process over time p [59, 85] is defined as

$$\frac{\partial H(p)}{\partial p} = -\hat{\mathcal{L}} H(p). \quad (4)$$

where $H(p)$ is the fundamental solution representing the energy flowing through the network at time p . To avoid confusion, the environment time-step is denoted by t whilst p indicates the time variable related to the diffusion process. For each pair of nodes u and v , the corresponding heat kernel entry

is given by

$$H(p)_{u,v} = \phi \exp[\Lambda p] \phi^\top = \sum_{i=1}^V \exp[-\lambda_i p] \phi_i(u) \phi_i(v) \quad (5)$$

where $H(p)_{u,v}$ quantifies the amount of heat that started in u and reached v at time p . In practice, Eq. (5) is approximated using Padé approximant [86],

$$H(p) = \exp[-p\hat{\mathcal{L}}]. \quad (6)$$

A useful property of $H(p)$ is that it is differentiable with respect to neural network parameters that define the Laplacian. This allows us to train an architecture where all the relevant quantities are estimated end-to-end via backpropagation. Additional details are provided in Section A.

We leverage this information to develop an attention mechanism that identifies the most important messages within the system, given the current graph topology. First, for every pair of nodes, we identify the critical time point \hat{p} at which the heat transfer drops by a pre-determined percentage δ and becomes stable, i.e. for each pair of u and v , we identify that critical value $\hat{p}(u, v)$ such that

$$\left| \frac{H^t(p+1)_{u,v} - H^t(p)_{u,v}}{H^t(p)_{u,v}} \right| < \delta. \quad (7)$$

In practice, the search of these critical values is carried out over a uniform grid of points. Once these critical time points are identified, we use them to evaluate the HK values, and arrange them into an $N \times N$ matrix,

$$H_{u,v}^t = H^t(\hat{p}(u, v))$$

which is used to define a multi-agent message-passing mechanism. Specifically, the final information content (or message) for an agent u is determined by a linear combination of the local messages received from all other agents,

$$\mathbf{m}_u^t = \sum_{v \in V} H_{u,v}^t \mathbf{c}_{u,v}^t \quad (8)$$

where the HK values are used to weight the importance of the incoming messages. Finally, the agent's action depends deterministically by its message,

$$a_u^t = \varphi_{\theta_u^p}(\mathbf{m}_u^t) \quad (9)$$

where $\varphi_{\theta_u^p}$ is a neural network with parameters θ_u^p . A lack of communication between a pair of agents results when no stable HK values can be found. In such cases, for a pair of agents (u, v) , the corresponding entry in $H_{u,v}^t$ will be zero hence no value of $\hat{p}(u, v)$ satisfies Eq. 7.

3.4 Reinforcement learning algorithm

In this section, we describe how the reinforcement learning algorithm is trained in an end-to-end fashion. We extend the actor-critic framework [34] in which an actor produces actions and a critic provides feedback on the actors' moves. In our architecture, multiple actors, one per each agent, receive feedback from a single, centralised critic.

In the standard DDPG algorithm [35, 36], the actor $\mu_\theta : \mathcal{O} \mapsto \mathcal{A}$ and the critic $Q^{\mu_\theta} : \mathcal{O} \times \mathcal{A} \mapsto \mathbb{R}$ are parametrised by neural networks with the aim to maximize the expected return,

$$J(\theta) = \mathbb{E} \left[\sum_{i=1}^T r(\mathbf{o}^t, a^t) \right].$$

where θ is the set of parameters that characterise the return. The gradient $\nabla_\theta J(\theta)$ required to update the parameter vector θ is calculated as follows,

$$\nabla_\theta J(\theta) = \mathbb{E}_{\mathbf{o}^t \sim \mathcal{D}} [\nabla_\theta \mu_\theta(\mathbf{o}^t) \nabla_{a^t} Q^{\mu_\theta}(\mathbf{o}^t, a^t) |_{a^t = \mu_\theta(\mathbf{o}^t)}]. \quad (10)$$

whilst Q^{μ_θ} is obtained by minimizing the following loss,

$$L(\theta) = \mathbb{E}_{\mathbf{o}^t, a^t, r^t, \mathbf{o}^{t+1} \sim \mathcal{D}} [(Q^{\mu_\theta}(\mathbf{o}^t, a^t) - y)^2] \quad (11)$$

where

$$y = r^t + \gamma Q^{\mu'_\theta}(\mathbf{o}^{t+1}, a^{t+1}).$$

Here, $Q^{\mu'_\theta}$ is a target critic whose parameters are only periodically updated with the parameters of Q^{μ_θ} , which is utilised to stabilize the training.

Our developments follow the CLDE paradigm [20, 37, 47]. The critics are employed during learning, but otherwise only the actor and communication modules are used at test time. At training time, a centralised critic uses the observations and actions of all the agents to produce the Q values. In order to make the critic unique for all the agents and keep the number of parameters constant, we approximate our Q function with a recurrent neural network (RNN). We treat the observation/action pairs as a sequence,

$$\mathbf{z}_i^t = \text{RNN}(\mathbf{o}_i^t, a_i^t | \mathbf{z}_{i-1}^t) \quad (12)$$

where \mathbf{z}_i^t and \mathbf{z}_{i-1}^t are the hidden state produced for the i^{th} and $i-1^{th}$ agent, respectively. Upon all the observation and action pairs from all the N agents are available, we use the last hidden state \mathbf{z}_N^t to produce the Q -value:

$$Q(\mathbf{o}_1^t, \dots, \mathbf{o}_N^t, a_1^t, \dots, a_N^t) = \varphi_{\theta_Q}(\mathbf{z}_N^t) \quad (13)$$

where φ is a neural network with parameters θ_Q . The parameters of the i^{th} agent are adjusted to maximize the objective function $J(\theta_i) = \mathbb{E}[R_i]$ following

the direction of the gradient $J(\theta_i)$,

$$\nabla_{\theta_i} J(\theta_i) = \mathbb{E}_{\mathbf{o}_i^t, a_i^t, r^t, \mathbf{o}_i^{t+1} \sim \mathcal{D}} [\nabla_{\theta_i} \boldsymbol{\mu}_{\theta_i}(\mathbf{m}_i^t) \nabla_{a_i^t} Q(\mathbf{x})|_{a_i^t = \boldsymbol{\mu}_{\theta_i}(\mathbf{m}_i^t)}] \quad (14)$$

where $\mathbf{x} = (\mathbf{o}_1^t, \dots, \mathbf{o}_N^t, a_1^t, \dots, a_N^t)$ and Q minimizes the temporal difference error, i.e.

$$L(\theta_i) = \mathbb{E}_{\mathbf{o}_i^t, a_i^t, r^t, \mathbf{o}_i^{t+1} \sim \mathcal{D}} [(Q(\mathbf{x}) - y)^2] \quad (15)$$

where

$$y = r_i^t + \gamma Q(\mathbf{o}_1^{t+1}, \dots, \mathbf{o}_N^{t+1}, a_1^{t+1}, \dots, a_N^{t+1}). \quad (16)$$

The differentiability of the heat kernel operator allows the gradient in Eq. (14) to be evaluated. Since the actions are modelled by a neural network parametrised θ_u in Eq.(9), we have that

$$\nabla_{\theta_u} \boldsymbol{\mu}_{\theta_u}(\mathbf{m}_u^t) = \nabla_{\theta_u} \varphi_{\theta_u}(\mathbf{m}_u^t). \quad (17)$$

and from Eq.(8) the gradient is

$$\frac{\partial \varphi(\mathbf{m}_u^t)}{\partial \theta_u} = \frac{\partial \varphi \left(\sum_{v \in V} H_{u,v}^t \mathbf{c}_{u,v}^t \right)}{\partial \varphi_{\theta_u}} \quad (18)$$

$$= \sum_{v \in V} \frac{\partial \varphi(H_{u,v}^t \mathbf{c}_{u,v}^t)}{\partial \varphi_{\theta_u}} \quad (19)$$

$$= \sum_{v \in V} \left(\frac{\partial \varphi(H_{u,v}^t)}{\partial \varphi_{\theta_u}} \mathbf{c}_{u,v}^t + H_{u,v}^t \frac{\partial \varphi(\mathbf{c}_{u,v}^t)}{\partial \varphi_{\theta_u}} \right). \quad (20)$$

whilst the gradients of the HK values are

$$\frac{\partial \varphi(H_{u,v}^t)}{\partial \varphi_{\theta_u}} = \frac{\partial \varphi(H_{u,v}^t(\hat{p}))}{\partial \varphi_{\theta_u}} \quad (21)$$

$$= \frac{\partial(\exp[-\hat{p}\hat{\mathcal{L}}])}{\partial \varphi_{\theta_u}} \quad (22)$$

$$= \frac{\partial(\exp[-\hat{p}\frac{1}{\sqrt{D}}\mathcal{L}\frac{1}{\sqrt{D}}])}{\partial \varphi_{\theta_u}} \quad (23)$$

$$= \frac{\partial(\exp[-\hat{p}\frac{1}{\sqrt{D}}(\mathbf{D} - \mathbf{S})\frac{1}{\sqrt{D}}])}{\partial \varphi_{\theta_u}} \quad (24)$$

which is a composition of differentiable operations. The pseudo-code summarising the proposed learning algorithm is provided in Section B of the Appendix. The proposed architecture is summarised in Figure 1.

4 Experimental results

4.1 Environments

The performance of CDC has been assessed in four different environments. Three of them are commonly used swarm robotic benchmarks: *Navigation Control*, *Formation Control* and *Line Control* [87–89]. A fourth one, *Pack Control*, has been added to study a more challenging task. All the environments have been tested using the Multi-Agent Particle Environment [37, 90], which allows agents to move around in two-dimensional spaces with discretised action spaces. In *Navigation Control* the agents must move closer to all landmarks whilst avoiding collisions; in *Formation Control* and *Line Control* they must navigate in order to form a polygonal geometric shape centred around the landmark and position themselves along the straight line connecting the two landmarks, respectively; in *Dynamic Pack Control*, workers need to follow the leaders to occupy a landmark and then move to a different location. Further details are given in the Appendix, Section G.

For each environment we have tested two versions with different number of agents: a *basic* one focusing on solving the designed task when 3–4 agents are involved, and a *scalable* one to show the ability to succeed with 8–10 agents. The performance of competing MADRL algorithms has been assessed using a number of metrics: the *reward*, which quantifies how well a task has been solved (the higher the better); the *distance*, which indicates the amount of navigation carried out by the agents to solve the task (the lower the better); the number of *collisions*, which shows the ability to avoid collisions (the lower the better); the *time* required to solve the task (the lower the better); the *success rate*, defined as the number of times an algorithm has solved a task over the total number of attempts; and *caught targets*, which refers to the number of landmarks that the pack managed to reach. Illustrative videos showing CDC in action on the above environments can be found online ¹.

4.2 Implementation details and experimental Setup

For our experiments, we use neural networks with two hidden layers (64 each) to implement the graph generation modules (Eq. 2, 1) and the action selector in Eq. 9. The RNN described in Equation 12 is implemented as a long-short term memory (LSTM) network [91] with 64 units for the hidden state.

We use the Adam optimizer [92] with a learning rate of 10^{-3} for critic and 10^{-4} for policies. Similarly to [75, 89], we set $\theta_1 = \theta_2 = \dots = \theta_N$ in order to make the model invariant to the number of agents. The reward discount factor is set to 0.95, the size of the replay buffer to 10^6 , and the batch size to 1,024. At each iteration, we calculate the heat kernel over a finite grid of $P = 300$ time points, with a threshold for getting stable values set to $s = 0.05$. This value has been determined experimentally (see Section E of the Appendix). The number of time steps for episode, T , is set to 50 for all the environments,

¹<https://youtu.be/H9kMtrnvRCQ>

except for Navigation Control where is set to 25. For Formation Control, Line Control and Pack Control the number E of episodes is set to is set to 50,000 for the basic versions (30,000 for scalable versions), while for Navigation Control is set to 100,000 (30,000 for scalable versions).

All network parameters are updated every time 100 new samples are added to the replay buffer. Soft updates with target networks use $\tau = 0.01$. We adopt the low-variance gradient estimator Gumbel-Softmax for discrete actions in order to allow the back-propagation to work properly with categorical variable, which can truncate the gradient's flow. All the presented results are produced by running every experiment 5 times with different seeds (1,2001,4001,6001,8001) in order to avoid that a particular choice of the seed can significantly condition the final performance. Python 3.6.6 [93] with PyTorch 0.4.1 [94] is used as framework for machine learning and automatic differentiable computing. NetworkX 2.2 [95] has been used for graph analysis. Computations were mainly performed using Intel(R) Xeon(R) CPU E5-2650 v3 at 2.30GHz as CPU and GeForce GTX TITAN X as GPU. With this configuration, the proposed CDC in average took approximately 8.3 hours to complete a training procedure on environments with four agents involved.

4.3 Main results

We have compared CDC against several different baselines, each one representing a different way to approach the MA coordination problem: independent DDPG [35, 36], MADDPG [37], CommNet [21], MAAC [29], ST-MARL [75], When2Com [96] and TarMAC [28]. Independent DDPG provides the simplest baseline in that each agent works independently to solve the task. In MADDPG each agent has its own critic with access to combined observations and actions from all agents during learning. CommNet implements an explicit form of communication; the policies are implemented through a large neural network with some components of the networks shared across all the agents and others agent-specific. At every time-step each agent's action depends on the local observation, and on the average of all other policies (neural network hidden states), used as messages. MAAC is a state-of-the art method in which an attention mechanism guides the critics to select the information to be shared with the actors. ST-MARL uses a graph neural network to capture the spatio-temporal dependency of the observations and facilitate cooperation. Unlike our approach, the graph edges here represents the time-depending agents' relationships, and capture the spatial and temporal dependencies amongst agents. When2Com utilises an attentional model to compute pairwise similarities between the agents' observation encodings, which results in a fully connected graph that is subsequently sparsified by a thresholding operation. Afterwards, each agent uses the remaining similarities scores to weight its neighbor observations before producing its action. TarMac is a framework where the agents broadcast their messages and then select whom to communicate to by aggregating the received communications together through an attention mechanism. Differently from the methods above, CDC utilises graph structures to support

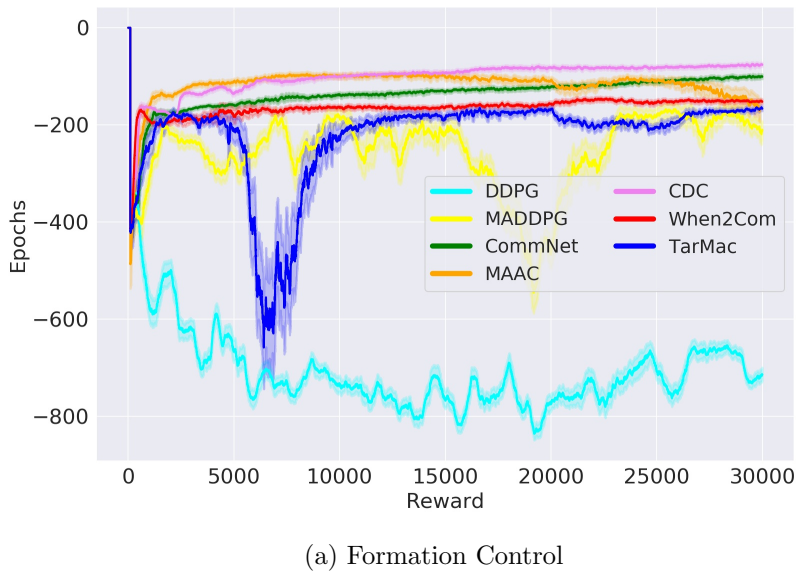
	Navigation Control $N = 3$			Navigation Control $N = 10$		
	Reward	# collisions	Distance	Reward	# collisions	Distance
DDPG	-57.3 \pm 9.94	1.24 \pm 0.39	4.09 \pm 6.92	-115.93 \pm 21.26	8.83 \pm 6.41	3.6 \pm 0.85
MADDPG	-45.23 \pm 6.59	0.77 \pm 0.24	3.16 \pm 5.74	-112.17 \pm 13.23	12.29 \pm 7.45	3.44 \pm 0.53
CommNet	-48.95 \pm 6.25	0.92 \pm 0.24	3.49 \pm 5.09	-104.49 \pm 10.45	12.21 \pm 6.87	3.14 \pm 0.41
MAAC	-43.18 \pm 6.44	0.71 \pm 0.24	1.46 \pm 2.97	-107.38 \pm 11.81	9.04 \pm 6.46	3.26 \pm 0.46
ST-MARL	-55.36 \pm 8.17	1.54 \pm 3.56	1.2 \pm 0.33	-110.69 \pm 15.75	32.73 \pm 32.77	3.27 \pm 0.57
When2Com	-40.7 \pm (5.33)	0.61 \pm (0.21)	1.06 \pm (3.26)	-112.51 \pm (14.48)	13.68 \pm (11.29)	3.45 \pm (0.57)
TarMAC	-44.9 \pm (6.22)	0.77 \pm (0.24)	2.14 \pm (4.36)	-110.67 \pm (13.76)	9.81 \pm (7.66)	3.39 \pm (0.54)
CDC	-39.16 \pm 4.77	0.56 \pm 0.19	0.4 \pm 1.66	-102.68 \pm 10.1	9.03 \pm 9.36	3.06 \pm 0.4
Formation Control $N = 4$						
	Reward	Time	Success Rate	Reward	Time	Success Rate
DDPG	-39.43 \pm 12.37	50 \pm 0.0	0 \pm 0.0	-49.27 \pm 6.11	50 \pm 0.0	0 \pm 0.0
MADDPG	-19.86 \pm 6.04	50 \pm 0.0	0 \pm 0.0	-20.65 \pm 7.11	50 \pm 0.0	0 \pm 0.0
CommNet	-7.77 \pm 2.06	45.8 \pm 10.19	0.18 \pm 0.38	-10.22 \pm 1.03	48.89 \pm 5.5	0.04 \pm 0.2
MAAC	-5.77 \pm 1.53	26.66 \pm 17.2	0.66 \pm 0.47	-9.63 \pm 1.35	50 \pm 0.0	0 \pm 0.0
ST-MARL	-20.24 \pm 3.0	50 \pm 0.0	0 \pm 0.0	-19.81 \pm 5.74	50 \pm 0.0	0 \pm 0.0
When2Com	-17 \pm (4.16)	48.21 \pm (10.11)	0.12 \pm (0.31)	-18.49 \pm (1.23)	48.72 \pm (0.9)	0.01 \pm (0.1)
TarMAC	-14.25 \pm (2.58)	47.35 \pm (12.87)	0.13 \pm (0.45)	-19.06 \pm (1.23)	49.44 \pm (5.6)	0.01 \pm (0.1)
CDC	-4.22 \pm 1.46	11.82 \pm 5.49	0.99 \pm 0.12	-7.51 \pm 1.06	15.21 \pm 9.23	0.99 \pm 0.1
Line Control $N = 4$						
	Reward	Time	Success Rate	Reward	Time	Success Rate
DDPG	-33.45 \pm 10.58	49.99 \pm 0.22	0 \pm 0.0	-68.19 \pm 10.2	50 \pm 0.0	0 \pm 0.0
MADDPG	11.55 \pm 2.79	47.32 \pm 9.14	0.08 \pm 0.27	-12.69 \pm 2.11	48.48 \pm 7.12	0.04 \pm 0.21
CommNet	-10.99 \pm 2.24	46.97 \pm 8.93	0.12 \pm 0.33	-9.58 \pm 1.28	37.73 \pm 14.85	0.47 \pm 0.5
MAAC	-7.38 \pm 2.09	17.08 \pm 12.17	0.89 \pm 0.32	-8.58 \pm 1.52	22.55 \pm 16.09	0.76 \pm 0.43
ST-MARL	-23.87 \pm 7.77	50 \pm 0.0	0 \pm 0.0	-19.24 \pm 6.26	50 \pm 0.0	0 \pm 0.0
When2Com	-16.45 \pm (3.01)	46 \pm (0.0)	0.11 \pm (0.3)	-10.1 \pm (2.8)	49.55 \pm 4.24	0.01 \pm (0.12)
TarMAC	-17.75 \pm (4.24)	47 \pm (0.0)	0.09 \pm (0.31)	-11.83 \pm (1.63)	49.91 \pm 1.12	0.01 \pm (0.09)
CDC	-5.97 \pm 1.73	10.42 \pm 5.58	0.98 \pm 0.13	-7.96 \pm 1.19	15.06 \pm 12.02	0.91 \pm 0.29
Dynamic Pack Control $N = 4$						
	Reward	Distance	Targets caught	Reward	Distance	Targets caught
DDPG	-224.77 \pm 87.65	3.52 \pm 1.67	0 \pm 0.0	-279.67 \pm 70.18	4.58 \pm 1.4	0 \pm 0.0
MADDPG	-116.15 \pm 71.37	1.46 \pm 0.72	0.2 \pm 0.13	-110.86 \pm 28.66	1.22 \pm 0.28	0.0 \pm 0.05
CommNet	293.35 \pm 446.89	1.11 \pm 0.12	0.81 \pm 0.89	-76.18 \pm 138.73	1.13 \pm 0.25	0.07 \pm 0.28
MAAC	-95.29 \pm 61.65	1.25 \pm 0.21	0.01 \pm 0.12	-105.15 \pm 46.42	1.15 \pm 0.28	0.01 \pm 0.09
ST-MARL	-107.02 \pm 71.84	1.26 \pm 0.3	0.02 \pm 0.14	-123.91 \pm 16.89	1.42 \pm 0.36	0 \pm 0.0
When2Com	-108.47 \pm (73.58)	1.32 \pm (0.33)	0.02 \pm (0.14)	-111.47 \pm (73.58)	1.32 \pm (0.33)	0.02 \pm (0.14)
TarMAC	50.47 \pm (73.58)	1.20 \pm 0.21	0.3 \pm 0.55	-78.18 \pm 42.5	1.18 \pm 0.76	0.05 \pm 0.21
CDC	369.5 \pm 463.92	1.09 \pm 0.1	0.96 \pm 0.93	58.03 \pm 279.05	1.12 \pm 0.14	0.35 \pm 0.56

Table 1: Comparison of DDPG, MADDPG, CommNet, MAAC, ST-MARL, When2Com, TarMAC and CDC on all four environments and using two different number of agents in each case. Results are averaged over five different seeds.

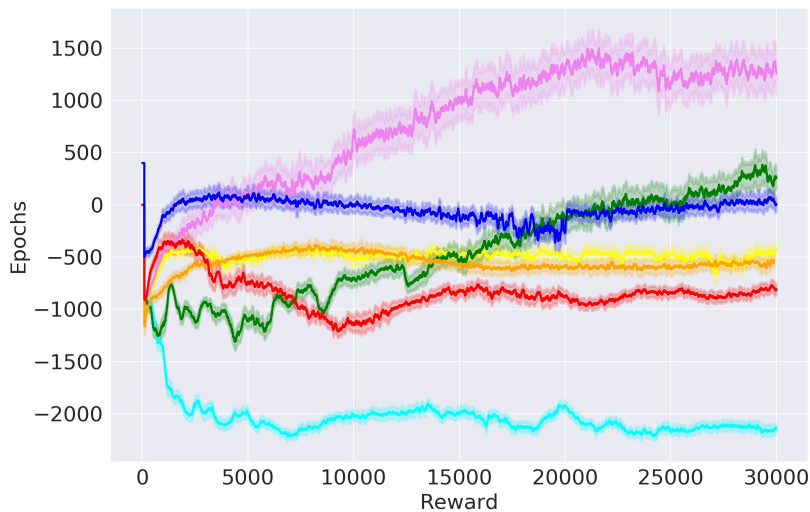
the formation of communication connectivities and then use the heat kernel, as an alternative form of attention mechanism, to allow to each agent to aggregate the messages coming from the others.

Table 1 summarises the experimental results obtained from all algorithms across all the environments. The metric values are obtained by executing the best model (chosen according to the best average reward returned during training) for an additional 100 episodes. We repeated each experiment using 5 different seeds, and each entry of Table 1 is an average over 500 values. It can be noted that CDC outperforms all the competitors on all four environments on all the metrics. In Navigation Control ($N = 3$), the task is solved by minimizing the overall distance travelled and the number of collisions, with an improvement over MAAC. In Formation Control ($N = 4$), the best performance is also achieved by CDC, which always succeeded in half of time compared to MAAC.

When the number of agents is increased, and the level of difficulty is significantly higher, all the baselines fail to complete the task whilst CDC still maintains excellent performance with a success rate of 0.99. In Line Control,



(a) Formation Control



(b) Dynamic Pack Control

Fig. 2: Learning curves for all the comparison algorithms on Formation Control (a) and Dynamic Pack Control (b). The x-axis the number of episodes and the y-axis the achieved rewards. All the results are averaged over five different runs.

both scenarios ($N = 4$ and $N = 10$) are efficiently solved by CDC with higher success rate and less time compared to MAAC, while all other algorithms fail. For Dynamic Pack Control, amongst the competitors, only CommNet does not fail. In this environment, only the leaders can see the point of interest, hence the other agents must learn how to communicate with them. In this case, CDC also outperforms CommNet on both the number of targets that are being caught and travelled distance. Overall, it can be noted that the gains in performance achieved by CDC, compared to other methods, significantly increase when increasing the number of agents.

Learning curves for Formation Control and Dynamic Pack Control, averaged over five runs, are shown in Figure 2 (see also the Appendix, Section C.1, for other environments). Here it can be noticed that CDC reaches the highest reward overall. The Dynamic Pack Control task is particularly interesting as only two methods are capable of solving it, CommNet and CDC, and both of them implement explicit communication mechanisms. With only 4 agents, the reward curves of CommNet, MAAC, When2Com, TarMac and CDC tend to be approximately similar, but increasing the numbers of agents to 8 highlights the remarkable benefits introduced by CDC. The high variance associated with CDC and CommNet in Dynamic Pack Control can be explained by the fact that, when a landmark is reached by all the agents, the environment returns a higher reward. These are the only two methods capable of solving the task, and lower variance is associated to other methods that perform poorly. The performance of CDC when varying the number of agents at execution time is investigated (see Appendix, Section H).

4.4 Communication analysis

In this section, we provide a qualitative evaluation of the communication patterns and associated topological structures that have emerged using CDC on the four environments. Figure 3 shows the communication networks G_H^t evolving over time at a given episode during execution: black circles represent the landmarks, blue circles indicate the normal agents, and the red circles are the leaders. Their coordinates within the two-dimensional area indicate the navigation trajectories. The lines connecting pairs of agents represent the time-varying edge weights, \mathbf{H}^t . Each $H_{u,v}^t$ element quantifies the amount of diffused heat between the two nodes, and Figure 3 illustrates how those quantities evolve over time. This figure can help identify which agents are involved in the communication at any given time.

As expected, different patterns emerge in different environments. Figure 3(a) shows that, in Formation Control, the dynamic graphs are highly connected in the early stages of the episodes, and are sparser later on when the formation is found. The degree of topological adjustment observed over time indicate initial bursts of communication activity at the beginning of an episode, while towards the end the communication mostly consists of messages shared across neighbours, which seems to be sufficient to maintain the

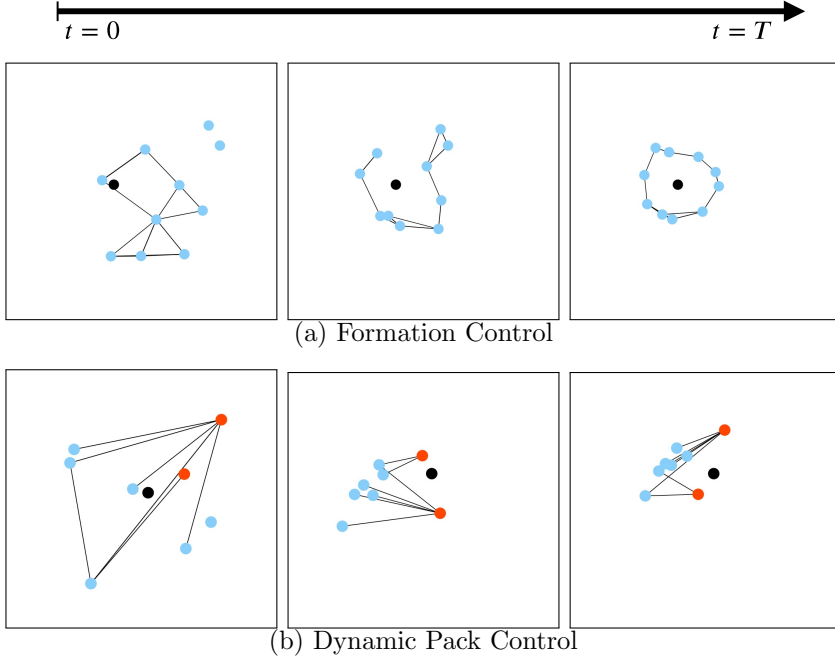


Fig. 3: Examples of communication networks G^t evolving over different episode time-steps on Formation Control and Dynamic Pack Control. Black circles represent landmarks; agents are represented in blue; in (b) red circles leader agents are indicated in red. Connections represent the stable heat kernel values utilised the environment changes in the communication process. It can be noted that different communication patterns are utilised on different environments. In (a) a circular pattern emerged to boost communication between neighbours, while in (b) the workers communicate with the leader to find the landmarks.

polygonal shape. A different situation can be observed in Dynamic Pack Control, in Figure 3(b). In this case, an intense communication activity emerges between leaders and members from an early stage, and the emerging topology approximates a bipartite graph between red and blue nodes. This is an expected and plausible pattern, given the nature of this environment. Solving this task requires that the leaders share information with the members, which otherwise would not know the landmark location. Patterns observed in other environments are reported in Section C.2.

Further appreciation for the role played by the heat kernel in driving the communication strategy can be gained by observing Figure 4 which provides visualisations for two environments (other environments are reported in Section C.3 of the Appendix). On the left, the connection weights are visualised using a circular layout. Here the nodes represent agents, and the size of

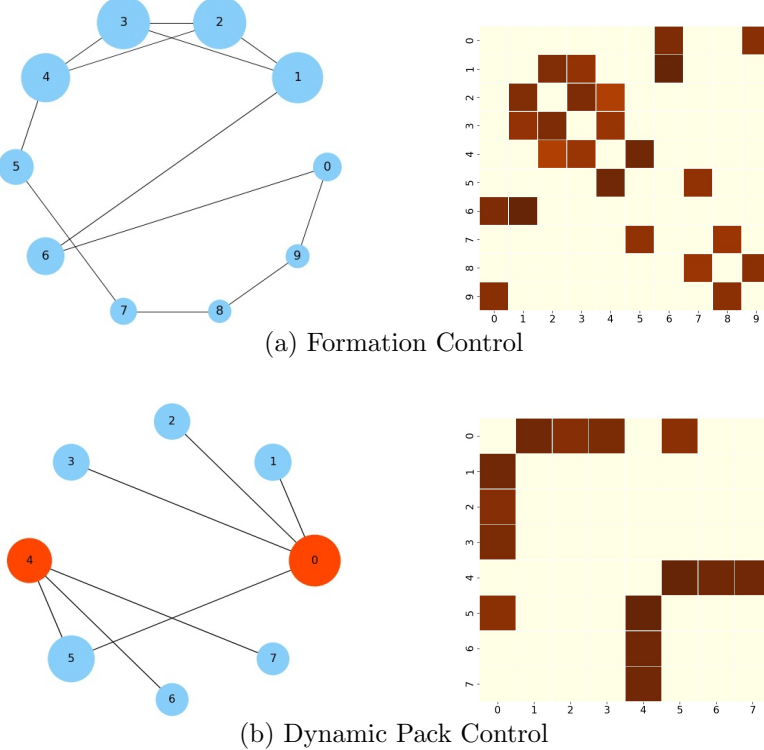


Fig. 4: Averaged communication graphs for (a) Formation Control and (b) Dynamic Pack Control. On the left, node sizes indicate the eigenvector centrality, where the connections the stable heat kernel values, while numbers the node labels. On the right, the heat kernel values are shown as heatmaps, where axis numbers correspond to node labels.

each node is proportional to the node's eigenvector centrality. The eigenvector centrality is a popular graph spectral measure [97], utilised to determine the influence of a node considering both its adjacent connections and the importance of its neighbouring node. This measure is calculated using the stable heat diffused values averaged over an episode, i.e. $H_{u,v} = (\sum_{t=1}^T H_{u,v}^t)/T$. The resulting graph structure reflects the overall communication patterns emerged while solving the given tasks. On the right, we visualise the squared $N \times N$ matrix of averaged pairwise diffusion values as a heatmap (red values are higher). It can be noted that, in Pack Control, two communities of agents are formed, each one with a leader. Here, as expected, leaders appear to be influential nodes (red nodes), and the heatmap shows that the connections between individual members and leaders are very strong. A different pattern emerges instead in Formation Control, where there is no evidence of communities since all nodes are connected to nearly form a circular shape. The corresponding

heatmap shows the heat kernel values connecting neighbouring agents tend to assume higher values compared to more distant agents.

5 Conclusions

In this work, we have presented a novel approach to deep multi-agent reinforcement learning that models agents as nodes of a state-dependent graph, and uses the overall topology of the graph to facilitate communication and cooperation. The inter-agent communication patterns are represented by a connectivity graph that is used to decide which messages should be shared with others, how often, and with whom. A key novelty of this approach is represented by the fact that the graph topology is inferred directly from observations and is utilised as an attention mechanism guiding the agents throughout the sequential decision process. Unlike other recently proposed architectures that rely on graph convolutional networks to extract features, but we make use of a graph diffusion process to simulate how the information propagates over the communication network and is aggregated. Our experimental results on four different environments have demonstrated that, compared to other state-of-the-art baselines, CDC can achieve superior performance on navigation tasks of increasing complexity, and remarkably so when the number of agents increases. We have also found that visualising the graphs learnt by the agents can shed some light on the role played by the diffusion process in mediating the communication strategy that ultimately yields highly rewarding policies.

This work represents an initial attempt to leverage well-known graph-theoretical properties in the context of a multi-agent communication strategy, and paves the way for future exploration along related directions. For instance, further constraints could be imposed on the graph edges to regulate the overall communication process, e.g. using a notion of flow conservation [98]. Further investigations could be directed towards the effects of adopting a decentralised critic modelling the communication content together with the agents' state-action values to provide a richer individual feedback.

Appendix

Appendix A Heat kernel: additional details

The heat kernel is a technique from spectral geometry [62], and is a fundamental solution of the *heat equation*:

$$\frac{\partial H^t(p)}{\partial p} = -\hat{\mathcal{L}}^t H^t(p). \quad (\text{A1})$$

Given a graph G defined on n vertices, the normalized Laplacian $\hat{\mathcal{L}}$, acting on functions with Neumann boundary conditions [99], is associated with the rate

of heat dissipation. $\hat{\mathcal{L}}$ can be written as:

$$\hat{\mathcal{L}} = \sum_{i=0}^{n-1} \lambda_i I_i \quad (\text{A2})$$

where I_i is the projection onto the i^{th} eigenfunction ϕ_i . For a given time $t \geq 0$, the heat kernel $H(t)$ is defined as a $n \times n$ matrix:

$$H(t) = \sum_i \exp[-\lambda_i t] I_i = \exp[-t \hat{\mathcal{L}}]. \quad (\text{A3})$$

Eq. A3 represents an analytical solution to Eq. A1.

Lemma 1 [59] The heat kernel $H(t)$ for a graph G with eigenfunctions θ_i satisfies:

$$H(t)_{u,v} = \sum_{i=1} \exp[-\lambda_i t] \phi_i(u) \phi_i(v) \quad (\text{A4})$$

The proof follows from the fact that

$$H(t) = \sum_i \exp[-\lambda_i t] I_i \quad (\text{A5})$$

and

$$I(u, v) = \phi_i(u) \phi_i(v). \quad (\text{A6})$$

Lemma 1 is provided to explain Eq. 5.

Appendix B Pseudo-code

Algorithm 1 CDC

```

1: Inizialise actor  $(\mu_{\theta_1}, \dots, \mu_{\theta_N})$  and critic networks  $(Q_{\theta_1}, \dots, Q_{\theta_N})$ 
2: Inizialise actor target networks  $(\mu'_{\theta_1}, \dots, \mu'_{\theta_N})$  and critic target networks
    $(Q'_{\theta_1}, \dots, Q'_{\theta_N})$ 
3: Inizialise replay buffer  $\mathcal{D}$ 
4: for episode = 1 to E do
5:   Reset environment,  $\mathbf{o}^1 = \mathbf{o}_1^1, \dots, \mathbf{o}_N^1$ 
6:   for t = 1 to T do
7:     Generate  $\mathbf{C}^t$  (Eq. 1) and  $\mathbf{S}^t$  (Eq. 2)
8:     for p = 1 to P do
9:       Compute Heat Kernel  $H(p)^t$  (Eq. 4)
10:      end for
11:      Build  $\mathbf{H}^t$  with stable Heat Kernel values (Eq. 7 )
12:      for agent i = 1 to N do
13:        Produce agent's message  $\mathbf{m}_i^t$  (Eq. 8)
14:        Select action  $a_i^t = \mu_{\theta_i}(\mathbf{m}_i^t)$ 
15:      end for
16:      Execute  $\mathbf{a}^t = (a_1^t, \dots, a_N^t)$ , observe r and  $\mathbf{o}^{t+1}$ 
17:      Store transaction  $(\mathbf{o}^t, \mathbf{a}^t, r, \mathbf{o}^{t+1})$  in  $\mathcal{D}$ 
18:    end for
19:    for agent i = 1 to N do
20:      Sample minibatch  $\Theta$  of  $B$  transactions  $(\mathbf{o}, \mathbf{a}, r, \mathbf{o}')$ 
21:      Update critic by minimizing:
22:
23:      
$$L(\theta_i) = \frac{1}{B} \sum_{(\mathbf{o}, \mathbf{a}, r, \mathbf{o}') \in \Theta} (y - Q(\mathbf{o}, \mathbf{a}))^2,$$

24:      where  $y = r_i + \gamma Q(\mathbf{o}', \mathbf{a}')|_{a_k' = \mu'_{\theta_k}(\mathbf{m}'_k)}$ 
25:      in which  $\mathbf{m}'_k$  is global message computed using target networks
26:      Update actor according to the policy gradient:
27:      
$$\nabla_{\theta_i} J \approx \frac{1}{B} \sum \left( \nabla_{\theta_i} \mu_{\theta_i}(\mathbf{m}_i) \nabla_{a_i} Q^{\mu_{\theta_i}}(\mathbf{o}, \mathbf{a})|_{a_i = \mu_{\theta_i}(\mathbf{m}_i)} \right)$$

28:    end for
29:    Update target networks:
30:    
$$\theta_i' = \tau \theta_i + (1 - \tau) \theta_i'$$

31: end for

```

Appendix C Additional results

C.1 Learning curves

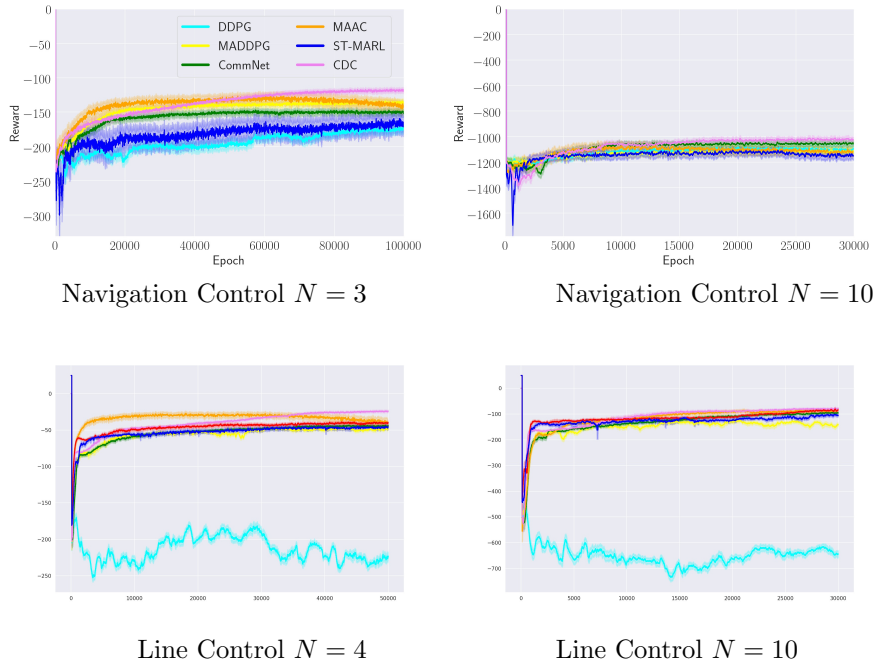


Fig. C1: Learning curves for 6 competing algorithms assessed on Navigation Control and Line Control. Horizontal axes report the number of episodes, while vertical axes the achieved rewards. Results are averaged over five different runs.

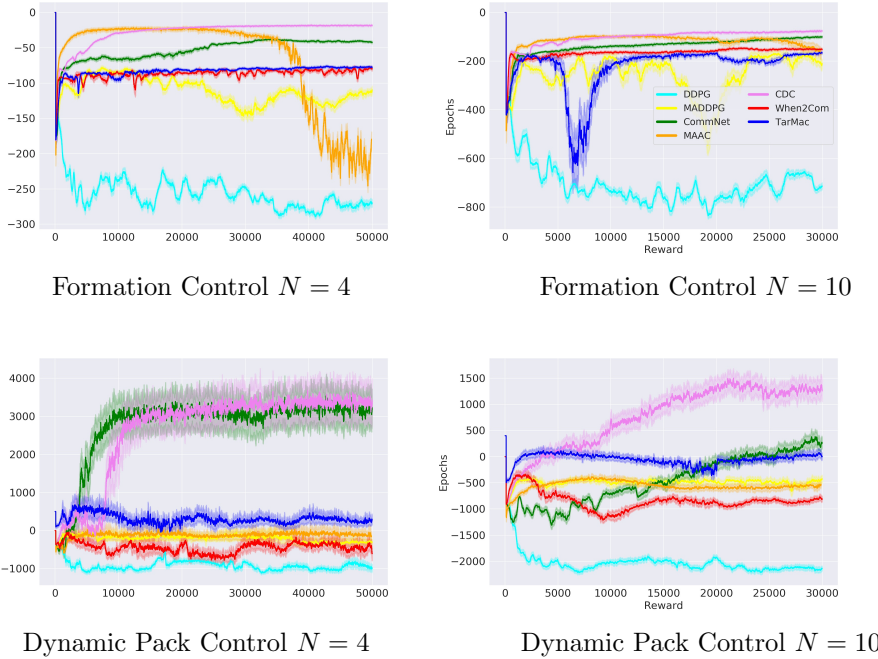


Fig. C2: Learning curves on Formation Control and Dynamic Pack Control. The horizontal axes report the number of episodes and vertical axes the achieved rewards. Results are averaged over five different runs.

C.2 Communication networks

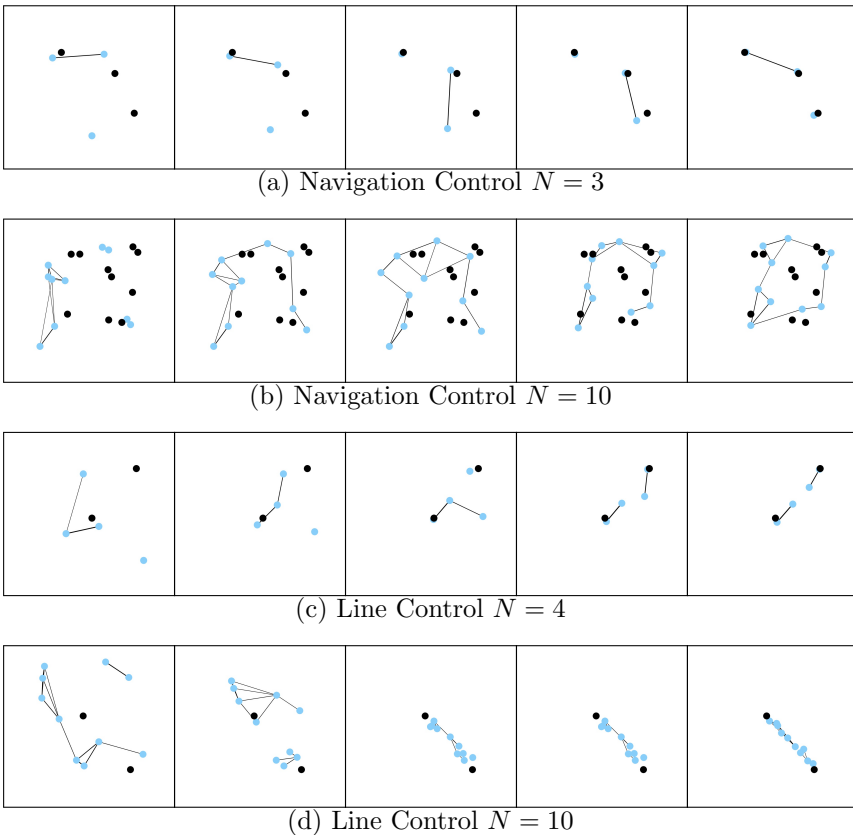


Fig. C3: Examples of communication networks G_H^t evolving over different episode time-steps.

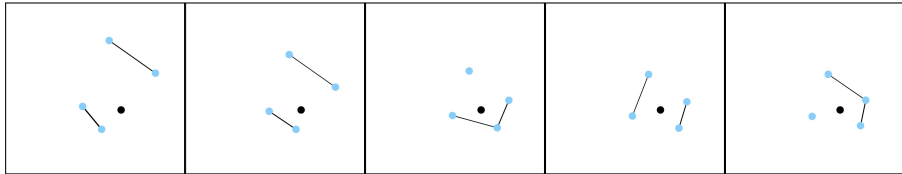
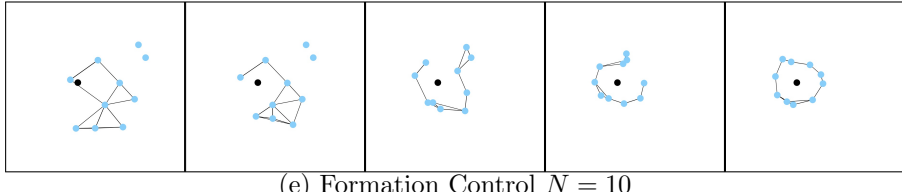
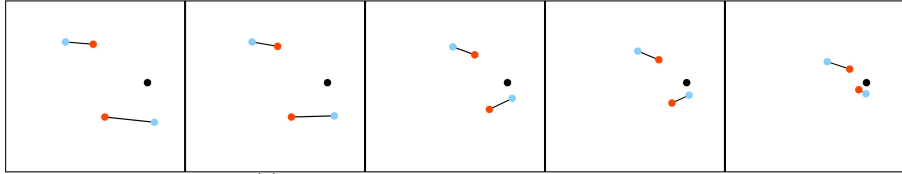
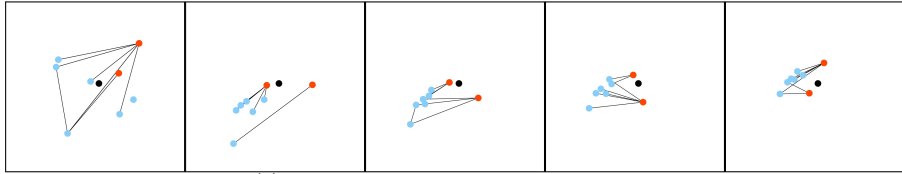
(e) Formation Control $N = 4$ (e) Formation Control $N = 10$ (f) Dynamical Pack Control $N = 4$ (f) Dynamical Pack Control $N = 4$

Fig. C4: Illustrations of communication networks G_H^t evolving over different episode time-steps.

C.3 Average communication graphs

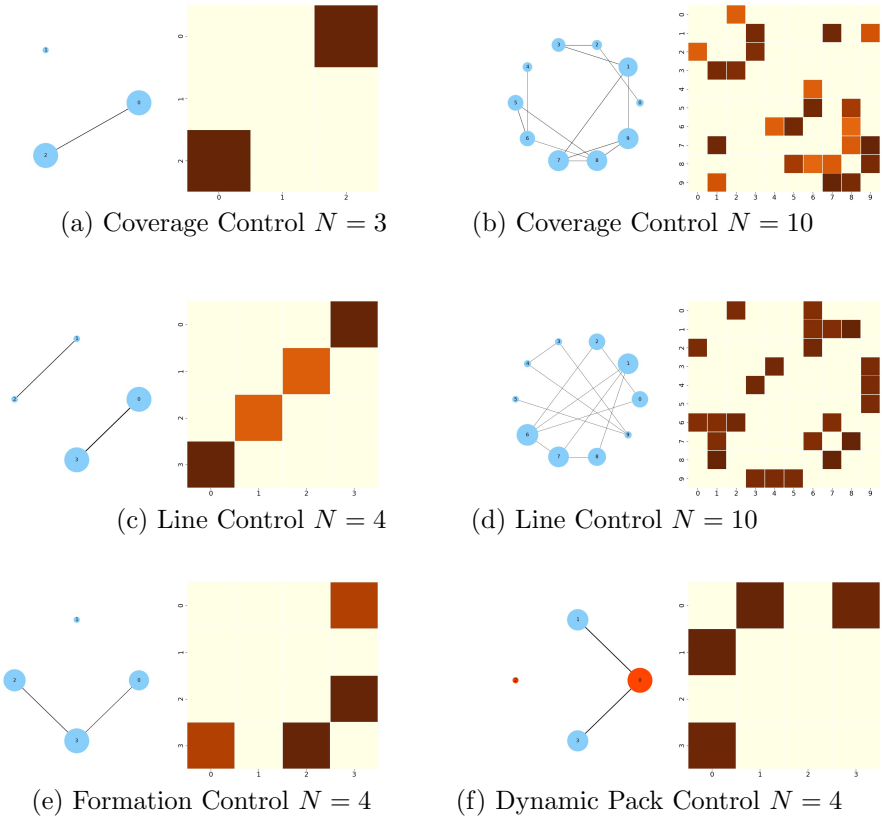


Fig. C5: Communication graphs averaged over an episode. For each environment, on the left, node sizes indicate the eigenvector centrality, connections the stable heat kernel values, while numbers the node labels. Here, a circular layout is used to represent the graphs in order to provide an alternative view where connection patterns can result easier to detect. On the right, diffused values are shown as heatmaps, where axis numbers correspond to node labels.

Appendix D Ablation study

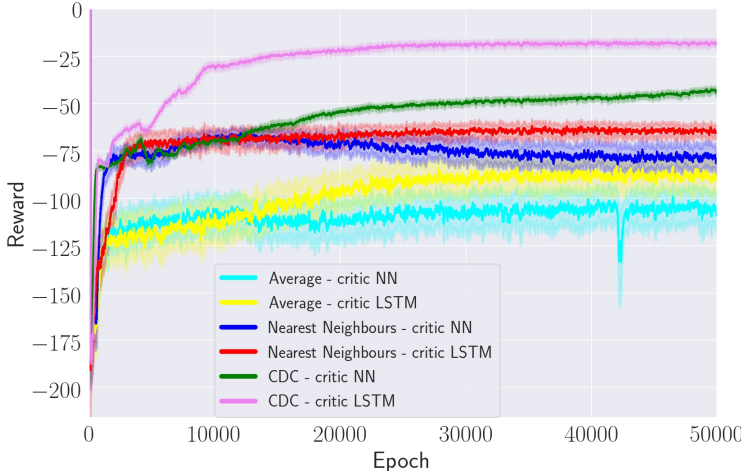


Fig. D6: Learning curves of different versions of the proposed model on Formation Control ($N = 4$).

In this section we present the results of an ablation study that has been carried out to investigate the specific benefits of the heat kernel over alternative and simpler information propagation mechanisms. In the *average* version, every agent takes an action after receiving an average of the observations of all other agents, whereas in the *nearest neighbours* version only the observations of an agent’s two nearest neighbours are averaged. For each one of these two mechanisms, we compare a version using the adopted critic (Section 3.4), which uses an RNN (specifically an LSTM), and the version using the traditional critic, which is based on a feed-forward neural network (NN). We also included results to investigate the effects of the LSTM critics on MADDPG.

In Figure D6, it can be noted that the heat kernel achieves the highest performance. Both versions of CDC, with LSTM and without, outperform the others. The results also show that the nearest neighbours version reaches better outcomes compared to the average version; this suggests that averaging all observations lead to noisier embeddings, and limits the effectiveness of the method. Overall, we have observed that using the LSTM-based critic leads to better performance overall. This result is somewhat expected given that the LSTM is able to filter out irrelevant information from a sequence of observations, and can retain only relevant information in its hidden state. From the obtained results, no significant differences have been observed upon changing the order of the agents in all the critic LSTM utilised.

Appendix E Choosing the heat kernel threshold

Method	Formation Control $N = 4$		
	Reward	Time	Success Rate
CDC $s = 0.01$	$-4.48 \pm (1.62)$	$13.52 \pm (9.83)$	$0.93 \pm (0.21)$
CDC $s = 0.025$	$-4.33 \pm (1.28)$	$14.01 \pm (9.74)$	$0.94 \pm (0.24)$
CDC $s = 0.05$	$-4.22 \pm (1.46)$	$11.82 \pm (5.49)$	$0.99 \pm (0.1)$
CDC $s = 0.075$	$-4.34 \pm (1.43)$	$12.88 \pm (9.13)$	$0.95 \pm (0.22)$
CDC $s = 0.1$	$-4.31 \pm (1.57)$	$12.52 \pm (8.39)$	$0.96 \pm (0.2)$

Table E1: Comparison of CDC results using different values for threshold s

Table E1 reports on the performance of CDC on Formation Control when the threshold parameter s varies over a grid of possible values (see Eq. 7). In turn, this threshold determines whether the heat kernel values are stable or not. The best performance is obtained using $s = 0.05$, which is the value used in all our experiments. To select the thresholds to test in Table E1, we defined a range of values close to solutions which have been proven to be successful in other heat kernel related works [33, 100].

Appendix F Varying the number of agents

# agents	DDPG	CDC
3	2.34 ± 0.61	1.06 ± 0.12
4	3.52 ± 1.67	1.09 ± 0.1
5	3.90 ± 1.68	1.08 ± 0.15
6	4.44 ± 1.7	1.08 ± 0.18
7	5.21 ± 1.98	1.12 ± 0.12
8	6.49 ± 2.17	1.13 ± 0.11

Table F2: Comparison of DDPG and CDC on Dynamic Pack Control. Both algorithms were trained with 4 agents and tested with 3-8. The performance metric used here is the distance of the the farthest agent to the landmark.

We tested whether CDC is capable of handling a different number of agents at test time. Table F2 shows how the performance of DDPG and CDC compares when they are both trained using 4 learners, but 3-8 agents are used at test time. We report on the maximum distance between the farthest agent and the landmark, which is invariant to the number of agents. It can be noted that CDC can handle systems with a varying number of agents, outperforming DDPG and keeping the final performance competitive with other methods that have been trained with a larger number of agents (see Table 1).

Appendix G Environment details

Navigation Control.

There are N agents and N fixed landmarks. The agents must move closer to all landmarks whilst avoiding collisions. Landmarks are not assigned to particular agents, and the agents are rewarded for minimizing the distances between their positions and the landmarks' positions. Each agent can observe the position of all the landmarks and other agents.

Formation Control.

There are N agents and only one landmark. In this scenario, the agents must navigate in order to form a polygonal geometric shape, whose shape is defined by the N agents, and centred around the landmark. The agents' objective is to minimize the distances between their locations and the positions required to form the expected shape. Each agent can observe the landmark only.

Line Control.

There are N agents and two landmarks. The agents must navigate in order to position themselves along the straight line connecting the two landmarks. Similarly to Formation Control, the agents objective is to minimize the distances between their locations and the positions required to form the expected shape. Each agent can observe the landmarks only.

Dynamic Pack Control.

There are N agents, of which two are leaders and $N - 2$ are members, and one landmark. The objective of this task is to simulate a pack behaviour, where agents have to navigate to reach the landmark. Once a landmark is occupied, it moves to a different location. The landmark location is accessible only to the leaders, while the members are blind, i.e. they can only see their current location.

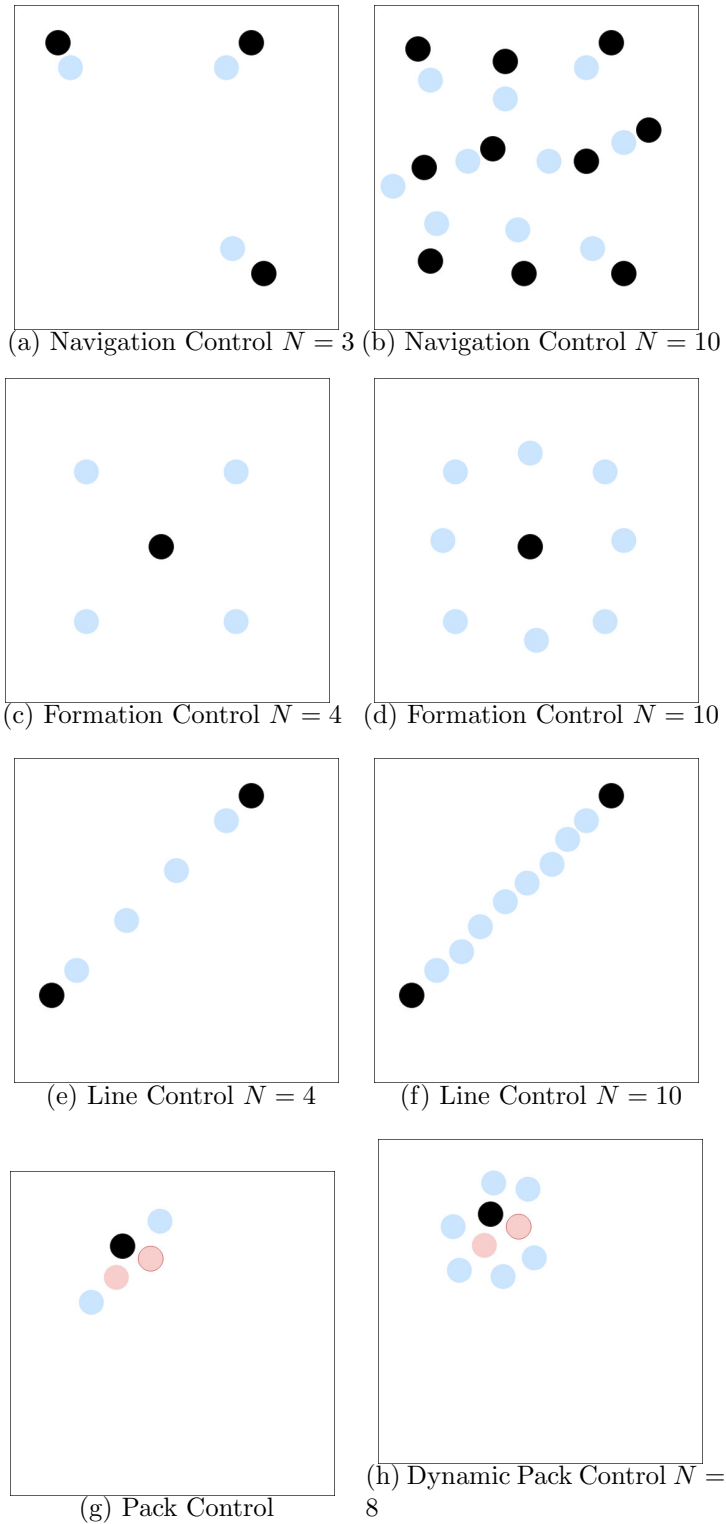


Fig. G7: Representations of all the utilised environments.

Appendix H Edge cutting example

Figure H8 shows the advantages of selecting edges by exploiting the heat kernel properties over a naive threshold approach. It can be noted that the heat diffusion considers not only the weight of an edge, but also its relevance within the graph structure. For example, a bridge that connects two communities is crucial importance for its function rather than its weight value.

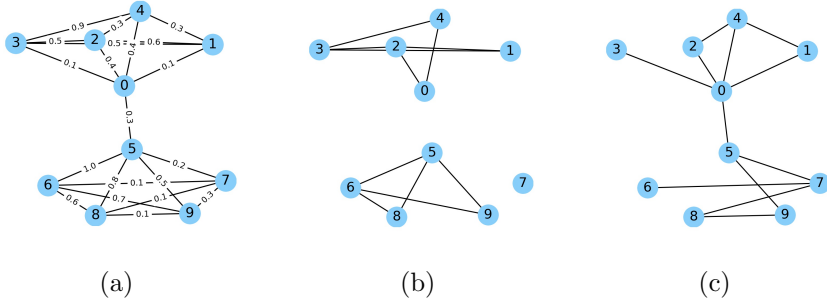


Fig. H8: An example of how different methods select important edges on a graph. The goal is to remove the less important connections considering both their weights and their structural role. (a) An input graph with edge weights in range $[0, 1]$. The connection between nodes 0-5 has a very important structural role, since it serves as bridge to connects two entire networks, despite having a weight relatively low (0.3). (b) Edges are selected using a threshold cutting based on the weights only (40th percentile). (c) Edge selection using a heat kernel approach; it can be noted that key edges, such as, the bridge, are preserved by the heat diffusion.

References

- [1] Sutton, R.S., Barto, A.G.: *Introduction to reinforcement learning*. MIT press Cambridge (1998)
- [2] LeCun, Y., Bengio, Y., Hinton, G.: Deep learning. *nature* **521**(7553), 436–444 (2015)
- [3] Schmidhuber, J.: Deep learning in neural networks: An overview. *Neural networks* **61**, 85–117 (2015)
- [4] Silver, D., Huang, A., Maddison, C.J., Guez, A., Sifre, L., Van Den Driessche, G., Schrittwieser, J., Antonoglou, I., Panneershelvam, V., Lanctot, M., *et al.*: Mastering the game of go with deep neural networks and tree search. *nature* **529**(7587), 484 (2016)

- [5] Mnih, V., Kavukcuoglu, K., Silver, D., Rusu, A.A., Veness, J., Bellemare, M.G., Graves, A., Riedmiller, M., Fidjeland, A.K., Ostrovski, G., et al.: Human-level control through deep reinforcement learning. *Nature* **518**(7540), 529 (2015)
- [6] Vinyals, O., Babuschkin, I., Czarnecki, W.M., Mathieu, M., Dudzik, A., Chung, J., Choi, D.H., Powell, R., Ewalds, T., Georgiev, P., et al.: Grandmaster level in starcraft ii using multi-agent reinforcement learning. *Nature*, 1–5 (2019)
- [7] Tanner, H.G., Kumar, A.: Towards decentralization of multi-robot navigation functions. In: Proceedings of the 2005 IEEE International Conference on Robotics and Automation, pp. 4132–4137 (2005). IEEE
- [8] Brunet, C.-A., Gonzalez-Rubio, R., Tetreault, M.: A multi-agent architecture for a driver model for autonomous road vehicles. In: Proceedings 1995 Canadian Conference on Electrical and Computer Engineering, vol. 2, pp. 772–775 (1995). IEEE
- [9] Dresner, K., Stone, P.: Multiagent traffic management: A reservation-based intersection control mechanism. In: Proceedings of the Third International Joint Conference on Autonomous Agents and Multiagent Systems-Volume 2, pp. 530–537 (2004). IEEE Computer Society
- [10] Lee, J.-H., Kim, C.-O.: Multi-agent systems applications in manufacturing systems and supply chain management: a review paper. *International Journal of Production Research* **46**(1), 233–265 (2008)
- [11] Hernandez-Leal, P., Kaisers, M., Baarslag, T., de Cote, E.M.: A survey of learning in multiagent environments: Dealing with non-stationarity. *arXiv preprint arXiv:1707.09183* (2017)
- [12] Rahaie, Z., Beigy, H.: Toward a solution to multi-agent credit assignment problem. In: 2009 International Conference of Soft Computing and Pattern Recognition, pp. 563–568 (2009). IEEE
- [13] Harati, A., Ahmadabadi, M.N., Araabi, B.N.: Knowledge-based multiagent credit assignment: A study on task type and critic information. *IEEE systems journal* **1**(1), 55–67 (2007)
- [14] Yliniemi, L., Tumer, K.: Multi-objective multiagent credit assignment through difference rewards in reinforcement learning. In: Asia-Pacific Conference on Simulated Evolution and Learning, pp. 407–418 (2014). Springer
- [15] Agogino, A.K., Tumer, K.: Unifying temporal and structural credit assignment problems. In: AAMAS, vol. 4, pp. 980–987 (2004)

- [16] Vorobeychik, Y., Joveski, Z., Yu, S.: Does communication help people coordinate? *PLoS one* **12**(2), 0170780 (2017)
- [17] Demichelis, S., Weibull, J.W.: Language, meaning, and games: A model of communication, coordination, and evolution. *American Economic Review* **98**(4), 1292–1311 (2008)
- [18] Miller, J.H., Moser, S.: Communication and coordination. *Complexity* **9**(5), 31–40 (2004)
- [19] Kearns, M.: Experiments in social computation. *Communications of the ACM* **55**(10), 56–67 (2012)
- [20] Foerster, J., Assael, I.A., de Freitas, N., Whiteson, S.: Learning to communicate with deep multi-agent reinforcement learning. In: *Advances in Neural Information Processing Systems*, pp. 2137–2145 (2016)
- [21] Sukhbaatar, S., Fergus, R., *et al.*: Learning multiagent communication with backpropagation. In: *Advances in Neural Information Processing Systems*, pp. 2244–2252 (2016)
- [22] Singh, A., Jain, T., Sukhbaatar, S.: Learning when to communicate at scale in multiagent cooperative and competitive tasks. *ICLR* (2019)
- [23] Pesce, E., Montana, G.: Improving coordination in multi-agent deep reinforcement learning through memory-driven communication. *Deep Reinforcement Learning Workshop, (NeurIPS 2018)*, Montreal, Canada (2019)
- [24] Jiang, J., Lu, Z.: Learning attentional communication for multi-agent cooperation. *arXiv preprint arXiv:1805.07733* (2018)
- [25] Mao, H., Zhang, Z., Xiao, Z., Gong, Z.: Modelling the dynamic joint policy of teammates with attention multi-agent ddpg. *arXiv preprint arXiv:1811.07029* (2018)
- [26] Liu, Y., Wang, W., Hu, Y., Hao, J., Chen, X., Gao, Y.: Multi-agent game abstraction via graph attention neural network. In: *AAAI*, pp. 7211–7218 (2020)
- [27] Hoshen, Y.: Vain: Attentional multi-agent predictive modeling. In: *Advances in Neural Information Processing Systems*, pp. 2701–2711 (2017)
- [28] Das, A., Gervet, T., Romoff, J., Batra, D., Parikh, D., Rabbat, M., Pineau, J.: Tarmac: Targeted multi-agent communication. *arXiv preprint arXiv:1810.11187* (2018)

- [29] Iqbal, S., Sha, F.: Actor-attention-critic for multi-agent reinforcement learning. ICML (2019)
- [30] Wang, T., Wang, J., Zheng, C., Zhang, C.: Learning nearly decomposable value functions via communication minimization. arXiv preprint arXiv:1910.05366 (2019)
- [31] Zhang, F., Hancock, E.R.: Graph spectral image smoothing using the heat kernel. Pattern Recognition **41**(11), 3328–3342 (2008)
- [32] Chung, A.W., Pesce, E., Monti, R.P., Montana, G.: Classifying hcp task-fmri networks using heat kernels. In: 2016 International Workshop on Pattern Recognition in NeuroImaging (PRNI), pp. 1–4 (2016). IEEE
- [33] Chung, A.W., Schirmer, M., Krishnan, M.L., Ball, G., Aljabar, P., Edwards, A.D., Montana, G.: Characterising brain network topologies: a dynamic analysis approach using heat kernels. Neuroimage **141**, 490–501 (2016)
- [34] Degris, T., White, M., Sutton, R.S.: Off-policy actor-critic. arXiv preprint arXiv:1205.4839 (2012)
- [35] Silver, D., Lever, G., Heess, N., Degris, T., Wierstra, D., Riedmiller, M.: Deterministic policy gradient algorithms. In: ICML (2014)
- [36] Lillicrap, T.P., Hunt, J.J., Pritzel, A., Heess, N., Erez, T., Tassa, Y., Silver, D., Wierstra, D.: Continuous control with deep reinforcement learning. CoRR **abs/1509.02971** (2015)
- [37] Lowe, R., Wu, Y., Tamar, A., Harb, J., Abbeel, O.P., Mordatch, I.: Multiagent actor-critic for mixed cooperative-competitive environments. In: Advances in Neural Information Processing Systems, pp. 6379–6390 (2017)
- [38] Stone, P., Veloso, M.: Multiagent systems: A survey from a machine learning perspective. Autonomous Robots **8**(3), 345–383 (2000)
- [39] Parsons, S., Wooldridge, M.: Game theory and decision theory in multiagent systems. Autonomous Agents and Multi-Agent Systems **5**(3), 243–254 (2002)
- [40] Shoham, Y., Leyton-Brown, K.: Multiagent systems: Algorithmic, game-theoretic, and logical foundations. Cambridge University Press (2008)
- [41] Nguyen, T.T., Nguyen, N.D., Nahavandi, S.: Deep reinforcement learning for multiagent systems: A review of challenges, solutions, and applications. IEEE transactions on cybernetics (2020)

- [42] Hernandez-Leal, P., Kartal, B., Taylor, M.E.: A survey and critique of multiagent deep reinforcement learning. *Autonomous Agents and Multi-Agent Systems* **33**(6), 750–797 (2019)
- [43] Albrecht, S.V., Stone, P.: Autonomous agents modelling other agents: A comprehensive survey and open problems. *Artificial Intelligence* **258**, 66–95 (2018)
- [44] Busoniu, L., Babuska, R., De Schutter, B.: A comprehensive survey of multiagent reinforcement learning. *IEEE Transactions on Systems, Man, and Cybernetics, Part C (Applications and Reviews)* **38**(2), 156–172 (2008)
- [45] Tuyls, K., Weiss, G.: Multiagent learning: Basics, challenges, and prospects. *Ai Magazine* **33**(3), 41 (2012)
- [46] Laurent, G.J., Matignon, L., Fort-Piat, L., *et al.*: The world of independent learners is not markovian. *International Journal of Knowledge-based and Intelligent Engineering Systems* **15**(1), 55–64 (2011)
- [47] Kraemer, L., Banerjee, B.: Multi-agent reinforcement learning as a rehearsal for decentralized planning. *Neurocomputing* **190**, 82–94 (2016)
- [48] Foerster, J., Farquhar, G., Afouras, T., Nardelli, N., Whiteson, S.: Counterfactual multi-agent policy gradients. *arXiv preprint arXiv:1705.08926* (2017)
- [49] Wang, R.E., Everett, M., How, J.P.: R-maddpg for partially observable environments and limited communication. *arXiv preprint arXiv:2002.06684* (2020)
- [50] Hochreiter, S., Schmidhuber, J.: Long short-term memory. *Neural computation* **9**(8), 1735–1780 (1997)
- [51] Lin, K., Zhao, R., Xu, Z., Zhou, J.: Efficient large-scale fleet management via multi-agent deep reinforcement learning. In: *Proceedings of the 24th ACM SIGKDD International Conference on Knowledge Discovery & Data Mining*, pp. 1774–1783 (2018)
- [52] Scardovi, L., Sepulchre, R.: Synchronization in networks of identical linear systems. In: *Decision and Control, 2008. CDC 2008. 47th IEEE Conference On*, pp. 546–551 (2008). IEEE
- [53] Wen, G., Duan, Z., Yu, W., Chen, G.: Consensus in multi-agent systems with communication constraints. *International Journal of Robust and Nonlinear Control* **22**(2), 170–182 (2012)

- [54] Wunder, M., Littman, M., Stone, M.: Communication, credibility and negotiation using a cognitive hierarchy model. In: Workshop# 19: MSDM 2009, p. 73 (2009)
- [55] Itō, T., Zhang, M., Robu, V., Fatima, S., Matsuo, T., Yamaki, H.: Innovations in Agent-Based Complex Automated Negotiations. Springer (2011)
- [56] Fox, D., Burgard, W., Kruppa, H., Thrun, S.: A probabilistic approach to collaborative multi-robot localization. *Autonomous robots* **8**(3), 325–344 (2000)
- [57] Peng, P., Yuan, Q., Wen, Y., Yang, Y., Tang, Z., Long, H., Wang, J.: Multiagent bidirectionally-coordinated nets for learning to play starcraft combat games. *arXiv preprint arXiv:1703.10069* (2017)
- [58] Vaswani, A., Shazeer, N., Parmar, N., Uszkoreit, J., Jones, L., Gomez, A.N., Kaiser, L., Polosukhin, I.: Attention is all you need. In: *Advances in Neural Information Processing Systems*, pp. 5998–6008 (2017)
- [59] Chung, F.R., Graham, F.C.: *Spectral graph theory*. American Mathematical Soc. (1997)
- [60] Brouwer, A.E., Haemers, W.H.: *Spectra of graphs*. Springer (2011)
- [61] Cvetkovic, D.M., DM, C., et al.: *Spectra of graphs. theory and application* (1980)
- [62] Schoen, R., Shing-Tung Yau Mack, C.A.: *Lectures on Differential Geometry*. International Press (1994)
- [63] Kloster, K., Gleich, D.F.: Heat kernel based community detection. In: *Proceedings of the 20th ACM SIGKDD International Conference on Knowledge Discovery and Data Mining*, pp. 1386–1395 (2014). ACM
- [64] Lafferty, J., Lebanon, G.: Diffusion kernels on statistical manifolds. *Journal of Machine Learning Research* **6**(Jan), 129–163 (2005)
- [65] Xu, B., Shen, H., Cao, Q., Cen, K., Cheng, X.: Graph convolutional networks using heat kernel for semi-supervised learning. *arXiv preprint arXiv:2007.16002* (2020)
- [66] Klicpera, J., Weißenberger, S., Günnemann, S.: Diffusion improves graph learning. In: *Advances in Neural Information Processing Systems*, pp. 13354–13366 (2019)
- [67] Kschischang, F.R., Frey, B.J., Loeliger, H.-A., et al.: Factor graphs and the sum-product algorithm. *IEEE Transactions on information theory*

47(2), 498–519 (2001)

[68] Kuyer, L., Whiteson, S., Bakker, B., Vlassis, N.: Multiagent reinforcement learning for urban traffic control using coordination graphs. In: Joint European Conference on Machine Learning and Knowledge Discovery in Databases, pp. 656–671 (2008). Springer

[69] Guestrin, C., Koller, D., Parr, R.: Multiagent planning with factored mdps. In: Advances in Neural Information Processing Systems, pp. 1523–1530 (2002)

[70] Liao, W., Bak-Jensen, B., Pillai, J.R., Wang, Y., Wang, Y.: A review of graph neural networks and their applications in power systems. arXiv preprint arXiv:2101.10025 (2021)

[71] Zhou, H., Ren, D., Xia, H., Fan, M., Yang, X., Huang, H.: Ast-gnn: An attention-based spatio-temporal graph neural network for interaction-aware pedestrian trajectory prediction. Neurocomputing 445, 298–308 (2021)

[72] Huang, Y., Bi, H., Li, Z., Mao, T., Wang, Z.: Stgat: Modeling spatial-temporal interactions for human trajectory prediction. In: Proceedings of the IEEE/CVF International Conference on Computer Vision, pp. 6272–6281 (2019)

[73] Mohamed, A., Qian, K., Elhoseiny, M., Claudel, C.: Social-stgcnn: A social spatio-temporal graph convolutional neural network for human trajectory prediction. In: Proceedings of the IEEE/CVF Conference on Computer Vision and Pattern Recognition, pp. 14424–14432 (2020)

[74] Xu, Z., Zhang, B., Bai, Y., Li, D., Fan, G.: Learning to coordinate via multiple graph neural networks. arXiv preprint arXiv:2104.03503 (2021)

[75] Wang, Y., Xu, T., Niu, X., Tan, C., Chen, E., Xiong, H.: Stmarl: A spatio-temporal multi-agent reinforcement learning approach for traffic light control. arXiv preprint arXiv:1908.10577 (2019)

[76] Li, S., Gupta, J.K., Morales, P., Allen, R., Kochenderfer, M.J.: Deep implicit coordination graphs for multi-agent reinforcement learning. arXiv preprint arXiv:2006.11438 (2020)

[77] Jiang, J., Dun, C., Huang, T., Lu, Z.: Graph convolutional reinforcement learning. arXiv preprint arXiv:1810.09202 (2018)

[78] Chen, H., Liu, Y., Zhou, Z., Hu, D., Zhang, M.: Gama: Graph attention multi-agent reinforcement learning algorithm for cooperation. Applied Intelligence 50(12), 4195–4205 (2020)

- [79] Seraj, E., Wang, Z., Paleja, R., Sklar, M., Patel, A., Gombolay, M.: Heterogeneous graph attention networks for learning diverse communication. arXiv preprint arXiv:2108.09568 (2021)
- [80] Su, J., Adams, S., Beling, P.A.: Counterfactual multi-agent reinforcement learning with graph convolution communication. arXiv preprint arXiv:2004.00470 (2020)
- [81] Yuan, Q., Fu, X., Li, Z., Luo, G., Li, J., Yang, F.: Graphcomm: Efficient graph convolutional communication for multi-agent cooperation. IEEE Internet of Things Journal (2021)
- [82] Niu, Y., Paleja, R., Gombolay, M.: Multi-agent graph-attention communication and teaming. In: Proceedings of the 20th International Conference on Autonomous Agents and MultiAgent Systems, pp. 964–973 (2021)
- [83] Littman, M.L.: Markov games as a framework for multi-agent reinforcement learning. In: Machine Learning Proceedings 1994, pp. 157–163. Elsevier, ??? (1994)
- [84] Kondor, R., Lafferty, J.: Diffusion kernels on graphs and other discrete input spaces. icml 2002. In: Proc, pp. 315–322 (2002)
- [85] Fiedler, M.: Laplacian of graphs and algebraic connectivity. Banach Center Publications **25**(1), 57–70 (1989)
- [86] Al-Mohy, A.H., Higham, N.J.: A new scaling and squaring algorithm for the matrix exponential. SIAM Journal on Matrix Analysis and Applications **31**(3), 970–989 (2009)
- [87] Mesbahi, M., Egerstedt, M.: Graph theoretic methods in multiagent networks. Princeton University Press (2010)
- [88] Balch, T., Arkin, R.C.: Behavior-based formation control for multirobot teams. IEEE transactions on robotics and automation **14**(6), 926–939 (1998)
- [89] Agarwal, A., Kumar, S., Sycara, K.: Learning transferable cooperative behavior in multi-agent teams. arXiv preprint arXiv:1906.01202 (2019)
- [90] Mordatch, I., Abbeel, P.: Emergence of grounded compositional language in multi-agent populations. arXiv preprint arXiv:1703.04908 (2017)
- [91] Schmidhuber, J.: A general method for multi-agent reinforcement learning in unrestricted environments. In: Adaptation, Coevolution and Learning in Multiagent Systems: Papers from the 1996 AAAI Spring

Symposium, pp. 84–87 (1996)

- [92] Kingma, D.P., Ba, J.: Adam: A method for stochastic optimization. arXiv preprint arXiv:1412.6980 (2014)
- [93] Van Rossum, G., Drake Jr, F.L.: Python tutorial. Centrum voor Wiskunde en Informatica Amsterdam, The Netherlands (1995)
- [94] Paszke, A., Gross, S., Chintala, S., Chanan, G., Yang, E., DeVito, Z., Lin, Z., Desmaison, A., Antiga, L., Lerer, A.: Automatic differentiation in PyTorch (2017)
- [95] Hagberg, A., Swart, P., S Chult, D.: Exploring network structure, dynamics, and function using networkx. Technical report, Los Alamos National Lab.(LANL), Los Alamos, NM (United States) (2008)
- [96] Liu, Y.-C., Tian, J., Glaser, N., Kira, Z.: When2com: Multi-agent perception via communication graph grouping. In: Proceedings of the IEEE/CVF Conference on Computer Vision and Pattern Recognition, pp. 4106–4115 (2020)
- [97] Bonacich, P.: Some unique properties of eigenvector centrality. Social networks **29**(4), 555–564 (2007)
- [98] Jia, J., Schaub, M.T., Segarra, S., Benson, A.R.: Graph-based semi-supervised & active learning for edge flows. In: Proceedings of the 25th ACM SIGKDD International Conference on Knowledge Discovery & Data Mining, pp. 761–771 (2019)
- [99] Cheng, A.H.-D., Cheng, D.T.: Heritage and early history of the boundary element method. Engineering Analysis with Boundary Elements **29**(3), 268–302 (2005)
- [100] Xiao, B., Wilson, R.C., Hancock, E.R.: Characterising graphs using the heat kernel. (2005)